Simulated ocean dynamics and lagrangian trajectory analysis in the Andaman Sea

Dwiky H. Abimanyu[1], *Muhammad* A. P. Sujiwo[2], *Agus* S. Atmadipoera[3*], *Nyoman* M. N. Natih[3]

[1]Marine Science and Technology Department, Faculty of Fisheries and Marine Sciences, IPB University, Bogor, Indonesia
[2]Advanced Research Laboratory (ARL), IPB University, Bogor, Indonesia
3Oceanographic Division, Department of Marine Science and Technology, IPB University, Bogor, Indonesia

Abstract. The Andaman Sea is a complex tropical basin significantly influenced by monsoonal forcing, which dictates regional circulation and water mass properties. This study utilizes a high-resolution (1/36º) CROCO ocean model and the Ichthyop Lagrangian tool to analyze circulation, thermohaline structure, and particle trajectories from 2015 to 2019. Findings indicate that monsoons drive substantial seasonal variability; the Northeast Monsoon promotes a northward flow of low-salinity water from the Malacca Strait, while the Southwest Monsoon facilitates saline Indian Ocean intrusion. Vertical analysis shows the thermocline fluctuating between 30 and 180 m, primarily influenced by Indian Ocean Dipole (IOD) events. EOF analysis revealed dominant annual periodicities of 341 days for temperature and salinity, while Lagrangian simulations identified particle retention along Sumatra during the Northeast Monsoon and westward export into the Indian Ocean during the Southwest Monsoon. Mean meridional volume transport was calculated at +0.32 Sv. These results provide a critical scientific basis for understanding regional biological connectivity and transboundary marine debris management in the Andaman region.

Keywords: Andaman Sea, ocean circulation, CROCO model, monsoonal variability, thermohaline structure.

1 Introduction

The Andaman Sea is a basin-shaped body of water bordered by Myanmar to the north, the Nicobar and Andaman Islands to the west, and Sumatra Island to the south [6]. In the southern part, the Andaman Sea is connected to the Strait of Malacca and influences the conditions of the strait (**Fig. 1**). The Strait of Malacca itself is a waterway that connects two large ocean regions situated between two landmasses, the island of Sumatra and the Malay Peninsula.

*Corresponding author: atmadipoera_itk@apps.ipb.ac.id

Water circulation in the Strait of Malacca is connected to the Indian Ocean and the South China Sea, making it highly influenced by the Indian Ocean Dipole (IOD) phenomenon [5].

The Andaman Sea is influenced by the tropical climate, specifically by the northeast monsoon and the southwest monsoon [8]. The northeast monsoon is characterized by cold and dry air from December to February, whereas the southwest monsoon is characterized by warm and dry conditions occurring from June to August [17]. Wind direction varies considerably during these monsoons; during the northeast monsoon, winds move from the north to the southwest, whereas during the southwest monsoon, winds move toward the northeast [9]. There is an exchange of material and water movement between the Andaman Sea and South China Sea through the Strait of Malacca. During the northeast monsoon, water currents from the South China Sea move toward the southern part of the Strait of Malacca and continue into the Andaman Sea [4]. During the southwest monsoon, water masses move from the Andaman Sea to the Strait of Malacca, carrying cold and saline water characteristics. The Strait of Malacca has a surface current that always flows northwestward toward the Andaman Sea. This is because the sea surface elevation in the southern part is consistently higher than that in the northern part [16].

Modeling is a numerical method used to simulate, analyze, and predict ocean dynamics, including ocean circulation, temperature-salinity variability, waves, and ocean-atmosphere interactions. This modeling approach is used to better understand the patterns of current circulation and the variability of Sea Surface Temperature (SST) and salinity in the Andaman Sea using reanalysis data built with the Coastal and Regional Ocean Community (CROCO) model. The CROCO model is a free-surface, hydrostatic, primitive equation model that has been integrated with the Modèle Aux Résolutions Spatiales 3D (MARS3D) and Hybrid Coordinate Ocean Model (HYCOM) [11].

Recent oceanographic studies on the Indonesian Maritime Continent have increasingly utilized CROCO because of its robust capability in resolving multi-scale processes in complex archipelagic domains. For example, recent applications in Indonesian Throughflow exit passages have demonstrated CROCO's effectiveness of CROCO in capturing high-frequency phenomena and vertical mixing. CROCO is based on the Regional Ocean Modeling System (ROMS) and SNH non-hydrostatic kernel. This model combines various oceanic parameters, such as biogeochemistry, physics, and ecological processes, to run simulations and analyze relationships within the marine ecosystem. Furthermore, CROCO can create predictive scenarios and perform data analysis for a given body of water.

Predictive scenarios run by the CROCO model simulation can be applied in several fields, such as determining the distribution patterns or trajectories of particles in waters with coastal and ocean current dynamics using Ichthyop. Ichthyop is a tool used to understand the relationship between physical and biological factors that influence larval dynamics [13]. This approach has been pivotal in recent fisheries management studies across the Indonesian archipelago to determine biophysical connectivity and design Marine Protected Areas (MPAs). Ichthyop can adapt the time-series data of temperature, salinity, and current velocity from the output of the CROCO model.

According to [15], the Ichthyop tool can also be used to track other trajectories, such as those of marine debris or microplastic particles, by adjusting its configuration. In the broader Indonesian region, such as the Java Sea, coupling hydrodynamic models with Ichthyop has successfully identified debris accumulation hotspots and transboundary pollution transport driven by monsoonal reversals. The goals of this study were to describe the ocean circulation in the Andaman Sea, describe the periodicity of sea surface temperature and salinity in the Andaman Sea, and analyze passive particle trajectories to aid in the understanding of ocean circulation and potential pollutant transport in the Andaman Sea.

2 Methods

2.1 Model configuration

The model domain is in the Andaman Sea, with an area of interest located at 93°E–101°E and 4°N–8.5°N, where the western boundary faces the Indian Ocean, to the Malaka Strait in the eastern boundary (**Fig. 1**).

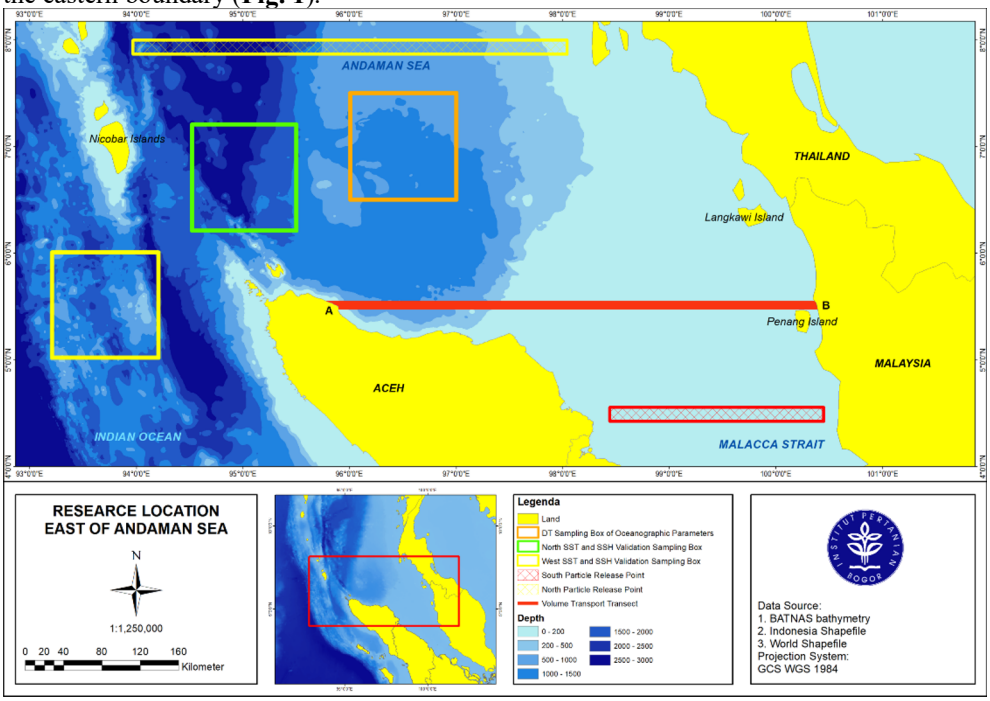

Fig. 1. Map of research site.

The general workflow for configuring and building an ocean-current simulation model typically consists of four main stages: data pre-processing, model setup and compilation, model execution, and visualization.

2.1.1 Data pre-processing

Data were input, and a general configuration for the Andaman Sea model was established within the crocotools_param.m file. The model domain data were located at 93°E to 101°E and 4°N to 8.5°N with 1/36º resolution. The model domain (or grid) was created in MATLAB using the make_grid command. The resulting grid dimensions, defined by LLm (grid points on the x-axis) and MMm (grid points on the y-axis), were saved in the parameter file. The bathymetric data used for the model were sourced from the GEBCO 15 arcsec dataset. The make_grid command in MATLAB was used to generate the grid file by integrating the bathymetry. The configurations of the parameters used to build the CROCO and Ichthyop models are presented in **Table 1** and **Table 2**.

Table 1. Configuration parameters for the CROCO ocean modeling system, including vertical stretching factors and depth constraints for the bathymetry.

Symbol	Description	Value
LLm	X grid	286
MMm	Y grid	162
N	Number of vertical levels	50
theta_s	Surface vertical stretching	6
theta_b	Bottom vertical stretching	0.1
H_c	Transition depth (meters)	10
H_{min}	Minimum depth (meters)	50
H_{max_coast}	Maximum depth at the coastal boundary (meters)	500
H_{max}	Maximum depth (meters)	5,000
DT	Time step model (seconds)	120
NDTFAST	Number of barotropic time steps per baroclinic time step	60
Format of the stored data		Daily
Simulation years		2015 to 2019
Spin-up year		2014
Simulation range		5 years

The make_OGCM_mercator command was executed to build the initial condition and open boundary condition data. The make_ERA5 command fetches and processes the required atmospheric data from the ERA5 dataset for use as an input in the CROCO simulation. Subsequently, the ERA5 data underwent a format conversion to make it compatible with CROCO's requirements of CROCO. The make-forcing command is executed to create atmospheric and oceanic forcing data. Finally, the last step in the CROCO pre-processing stage was to run the make_tides command, which was used to build the tidal component forcing.

Table 2. Model parameters and initial release coordinates for the particle-tracking simulation conducted via the Ichthyop platform.

Symbol	Description
Release point	98.441 – 100.449 ºE and 4.423 – 4.554 ºN
	93.965 – 98.04 ºE and 7.869 – 8 ºN
Simulation period (days)	87
Time step (seconds)	600
Number of particles	10.000
Coastal behavior	Beaching
Numerical advection scheme	Runge kutta 4
Turbulence dissipation rate (m^2/s^3)	1×10^{-9}

2.1.2 Model setup and compilation

After completing the preprocessing stage, the generated NetCDF files—croco_grd.nc (grid), croco_frc.nc (forcing), croco_bry.nc (boundary), croco_ini.nc (initial), and croco_clm.nc (climatology)— were used as inputs for the compilation stage. Adjustments to the grid values LLm and MMm, as well as the configuration name, were made using the param.h script. Following this, the cppdefs.h script was modified to select the appropriate C-preprocessor options for compiling the CROCO model. Finally, the data were compiled using the jobcomp script with the GNU Fortran compiler (GFORTRAN).

2.1.3 Model execution

The model running stage was the final stage of data processing in CROCO modeling. The next step involved adjusting several parameters in the croco_inter.in file. Subsequently, the model was executed using the run_croco_inter.bash command to run the model for an extended period. The model is driven by the input file resulting from croco_inter.in, and runs until it reaches statistical stability.

2.1.4 Visualization

The results from running the model consisted of croco average files (croco_avg.nc-Y2015M01 – croco_avg.nc-Y2019M12) and croco history files (croco_his.nc-Y2015M01 – croco_his.nc-Y2019M12), with the output in a merged NetCDF format. Subsequently, the results were visualized using JupyterLab, which uses the PyFerret programming language. Within JupyterLab, components such as zonal and meridional current velocity, temperature, salinity, and other derivative parameters can be displayed.

2.2 Data analysis

2.2.1 Depth-time plot

Temperature, salinity, zonal current (**u**), and meridional current (**v**) were analyzed using depth-time plots to observe changes in these parameters over time at depths from 0 to 300 m. The location for the analysis was determined by creating a spatial average within a 1º×1º sample box.

2.2.2 Annual cycle (climatology) analysis

The temperature parameter, overlaid with current vectors, is displayed at a depth of 0.5 m to visualize the distribution of temperature, salinity, and current values formed at that depth. Data were averaged into monthly values for a single year.

2.2.3 Empirical Orthogonal Function (EOF) analysis

Empirical Orthogonal Function (EOF) analysis is a method used to identify variations in spatial and temporal patterns from a time-series dataset (2015 to 2019). This method reduces a complex dataset to a simpler one [3]. According to [12], new variables with smaller dimensions are called EOF modes. The principle of EOF analysis is the decomposition of a time series signal into spatial and temporal functions.

2.2.4 Power Spectral Density (PSD) analysis

Power Spectral Density (PSD) analysis is used to estimate the spectral density function of a time-series dataset. This method identifies peaks in the current signal that possess sufficiently high energy, which is referred to as peak energy. This peak energy was derived from a specific time period with a 95% confidence interval, allowing for clear observations [1]. The dominant variability that may emerge from the time-series dataset includes intra-seasonal, semi-annual, annual, and inter-annual periodicities. According to [2], the PSD value is determined using the Fast Fourier Transform (FFT) method.

2.2.5 Volume transport

The water mass transport entering from the Strait of Malacca can be calculated by integrating the meridional current component over the length of transects A to B in longitude and the depth of the transect.

$$Qv = \int_B^A \int_z^0 v dz\, dx \quad (1)$$

Where Qv is the volume transport quantity (1 sverdrup = 10^6 m^3/s) across transects A–B, z is the depth of the lower boundary from the topography, and **v** is the meridional current component (m/s).

2.2.6 Trajectory analysis

Trajectory analysis was performed by releasing 10,000 passive particles into the northern and southern parts of the eastern Andaman Sea. The particles were given the property of becoming stuck upon encountering a coastline. This procedure was conducted in four stages. The first stage involved configuring the simulation for particle release and setting the particle properties. The second stage involved running the simulation. The third stage mapped the results of the completed simulation. The final stage involved creating an animation . gif format.

3 Results and discussion

3.1 Data validation

Validation of SST (**Fig. 2a**) showed strong agreement in the north (RMSD 0.835, SD 3.506, r=0.976) and west (RMSD 0.623, SD 3.546, r=0.988). Similarly, the SSH data (**Fig. 2b**) demonstrated high accuracy with an RMSD of 0.067 in both regions and correlations of 0.921 (north) and 0.941 (west). Supported by [18] and [19], the low RMSD values and correlations approaching 1 confirm the reliability of the model and its high consistency with satellite data.

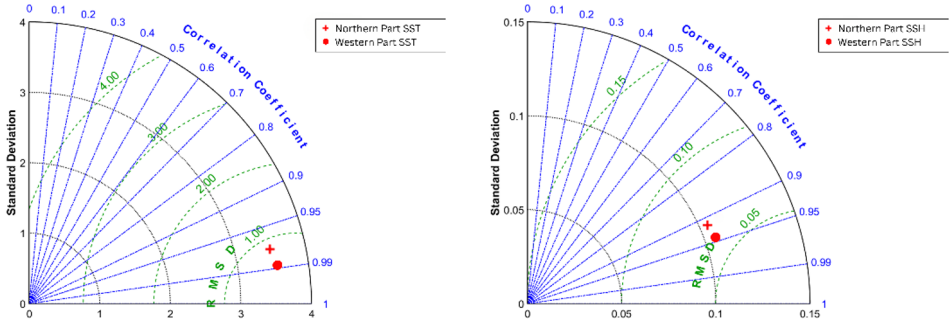

(a)

(b)

Fig. 2. Taylor diagrams providing a statistical validation of model anomaly data for (a) Sea Surface Temperature (SST) and (b) Sea Surface Height (SSH) at northern and western observation points. These diagrams facilitate a simultaneous evaluation of the correlation coefficients, Root Mean Square Difference (RMSD), and standard deviation, demonstrating the model's skill in replicating observed oceanic variability.

3.2 Depth-time fluctuation of oceanographic parameters

The oceanographic conditions in the Andaman Sea from 2015 to 2019, represented by temperature-depth-time plots (**Fig. 3**), show clear thermal fluctuations. The sea temperature decreases with depth, ranging from 10°C to 27°C between 0 and 300 m. The lowest surface temperature (~24.5°C) occurred in December 2019, shoaling the thermocline to 30–100 m. The highest surface temperature (~28.7°C) was observed in May 2016, deepening the thermocline to 80–180 m. These variations are linked to the Indian Ocean Dipole (IOD). A significant positive IOD event in 9 caused unusually low temperatures during the northeast monsoon, whereas a negative IOD event in 6 led to elevated temperatures during the southwest monsoon. These findings align with those of previous research [10], confirming the strong influence of the IOD on regional thermal anomalies. In 2016, a strong El Niño event was recorded in the Pacific Ocean. El Niño shifts the atmospheric convection (Walker Circulation) toward the central Pacific, usually causing upwelling or cooler SSTs around Indonesia. Because the observed data showed a record high (warming), it contradicts the typical signature of El Niño. Therefore, warming is dynamically driven by local IOD forcing (negative phase), which overpowers the residual El Niño signal. According to previous research [20], anomalous westerly winds piled warm water along the coast of Sumatra, leading to high SSTs in 2016.

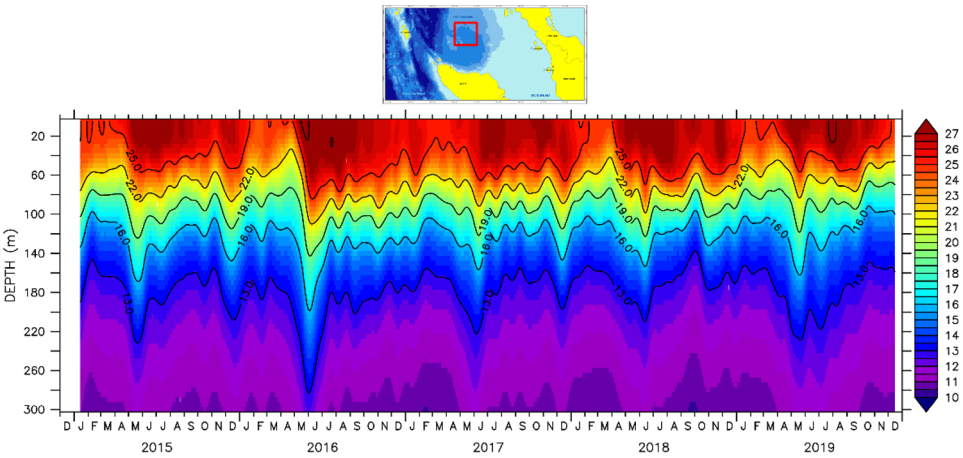

Fig. 3. Time-series vertical profile (Hovmöller diagram) of water temperature across the upper 300 meters of the water column from 2015 to 2019. The contour lines and color gradients illustrate the seasonal thermocline dynamics and interannual temperature variability within the study area indicated in the inset map.

Salinity measurements in the Andaman Sea (2015–2019) fluctuated most notably in the upper 70 m (**Fig. 4**), with values ranging from 31.82 to 35.07 psu. The lowest surface salinity (~31.8 psu) occurred in November 2017, deepening the barrier layer by 30–70 m. The highest surface salinity (~33.5 psu) was observed in March 2015, when the barrier layer was shoaled to 20–30 m. This variability was seasonally driven. During the southwest monsoon, high-salinity waters from the Northern Andaman Sea and Indian Ocean increase the salinity in the region. Conversely, the northeast monsoon transports low-salinity water from the Strait of Malacca, which is influenced by river runoff, into the Andaman Sea. These findings align with those of [14], confirming that reduced salinity is often linked to freshwater input from rivers.

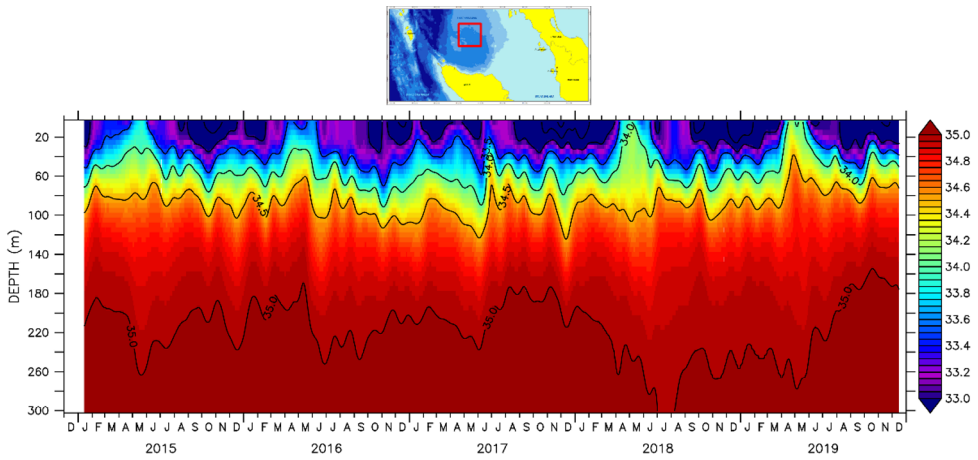

Fig. 4. Depth-time distribution of salinity levels from 2015 to 2019, showing the vertical haline structure from the surface to 300 meters depth. The plot visualizes fluctuations in salinity concentration over time, with the inset map indicating the specific geographic coordinate where these vertical profiles were extracted for the simulation.

The zonal currents in the Andaman Sea (2015–2019, 0–300 m depth) exhibited distinct monthly variability. During the northeast monsoon, the surface zonal currents showed negative values (blue), indicating a dominant westward flow. In contrast, the southwest monsoon displayed positive values (red), reflecting a predominantly eastward flow (**Fig. 5**). This seasonal reversal, driven by monsoon winds, affects the surface layer to depths of 80–150 m.

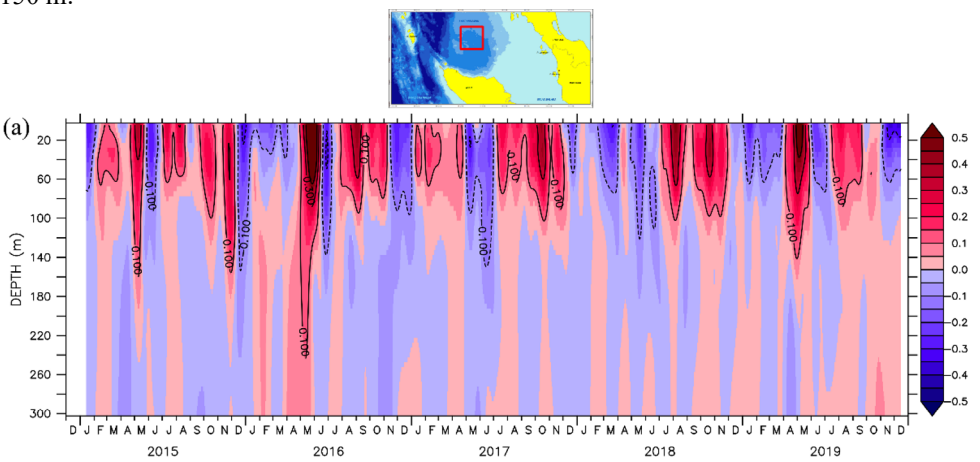

Fig. 5. Depth-time plot of zonal current velocity (*u*-component) across the upper 300 meters from 2015 to 2019. Positive values (red) indicate eastward flow while negative values (blue) indicate westward flow, revealing the seasonal and vertical shear patterns of the current system at the designated study location.

The meridional current in the Andaman Sea (2015–2019, 0–300 m depth) exhibited distinct monthly variations. During the southwest monsoon, surface meridional currents showed positive values (red), indicating dominant northward flow, whereas during the same monsoon period, surface currents also displayed negative values (blue), reflecting southward movement (**Fig. 6**). This pattern is driven by seasonal monsoon winds, which influence the current directions in the surface layer down to a depth of approximately 100 m.

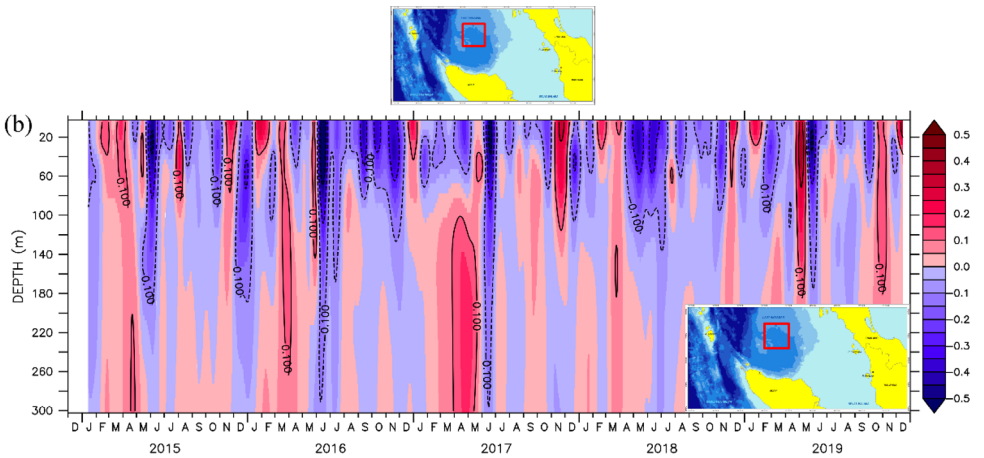

Fig. 6. Depth-time distribution of the meridional current velocity (*v*-component) from 2015 to 2019, showing the strength of northward (positive) and southward (negative) flow components. The profiles visualize the seasonal variability of current velocity in the upper 300 meters of the water column as specified in the geographic inset.

3.3 Annual cycle (climatology) of ocean circulation and SST

The temporal fluctuations in the current patterns and salinity presented in **Fig. 7** and **Fig. 8** are primarily driven by the seasonal reversal of the monsoonal system and the resulting hydrodynamic pressure gradients. The flow structure at 0.5 m depth varies significantly by season, and during the Northeast Monsoon, circulation is dominated by outflow from the Strait of Malacca, driven dynamically by the sea surface slope tilting toward the Andaman Sea [8]. Conversely, during the Southwest Monsoon, currents shift southward from the Northern Andaman Sea, while Indian Ocean waters move along Sumatra's west coast into the Strait of Malacca because of sea level differences between the Indian Ocean and the South China Sea [9]. This interaction of water masses—specifically the Indian Ocean inflow and strong Malacca Strait outflow during the transition month of April—generates distinct mesoscale features, including a cold-core cyclonic eddy at 6°N, 96°E and a warm-core anticyclonic eddy at 6.4°N, 97.5°E [7]. These circulation dynamics directly govern the salinity distribution, which ranges from lower values (32.2–33 psu) during the Northeast Monsoon, attributed to the influence of the Malacca Strait water, to higher values (33–33.4 psu) during the Southwest Monsoon as more saline Indian Ocean water intrudes into the region.

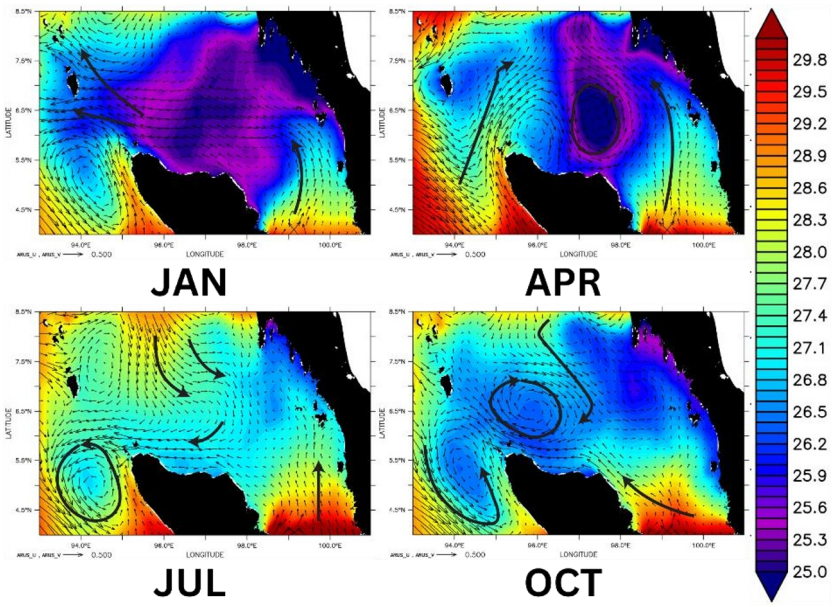

Fig. 7. Seasonal climatology of surface current patterns (arrows) overlaid with Sea Surface Temperature (SST, color shading) for the months of January, April, July, and October averaged from 2015 to 2019.

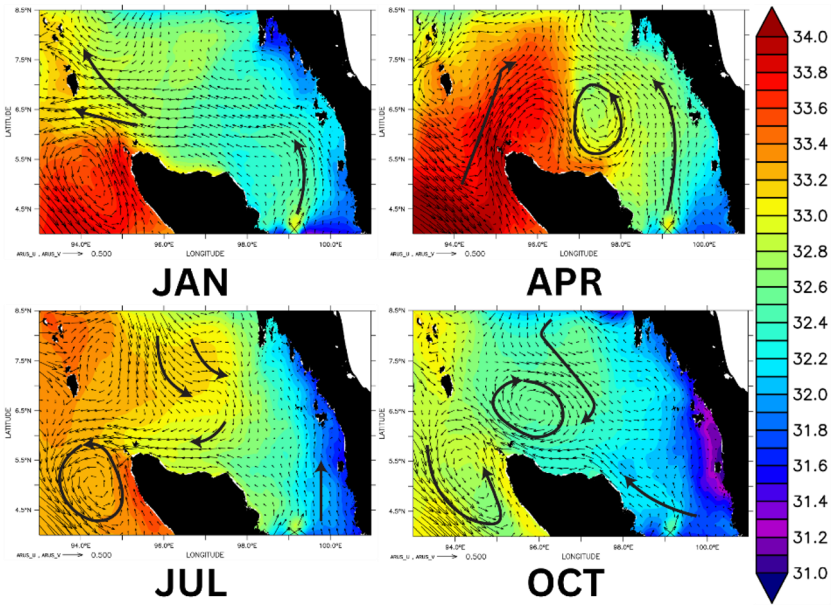

Fig. 8. Seasonal climatology of surface current patterns (vectors) overlaid with salinity (color shading) for January, April, July, and October averaged from 2015 to 2019.

3.4 Trajectory analysis

3.4.1 Northeastern moonson simulation

The filtered particle trajectory simulation for the northeast monsoon in the Andaman Sea revealed movement dominated by seasonal currents. The particles primarily drift northward in a counterclockwise rotating pattern owing to the influence of eddies. Initially, the particles advance northward in a spiral motion. They subsequently disperse toward Aceh, with some stalling upon reaching the coasts of Sumatra and the Malay Peninsula. Over time, the particles travel farther toward the Andaman and Nicobar Islands, eventually exiting the model domain. In the final phase, particles were widely dispersed across the Andaman Sea; some remained near the Malay Peninsula coast, while others drifted westward into the Indian Ocean. Particle temperatures, initially approximately 27°C, gradually decreased to 20–23°C over time.

Lagrangian particle trajectories have significant implications for ecosystem connectivity and environmental management. The observed coastal stalling along Sumatra and the Malay Peninsula identifies these shorelines as potential accumulation zones for marine debris during the Northeast Monsoon. Biologically, the temperature decrease of the particles from 27°C to 20–23°C, coupled with counterclockwise circulation, confirms the influence of cyclonic (cold-core) eddies. This suggests that these circulation features facilitate the transport of deep nutrient-rich water, potentially marking these zones as areas of high biological productivity. Furthermore, the eventual drift of particles into the wider Indian Ocean highlights the transboundary nature of the surface transport in this region.

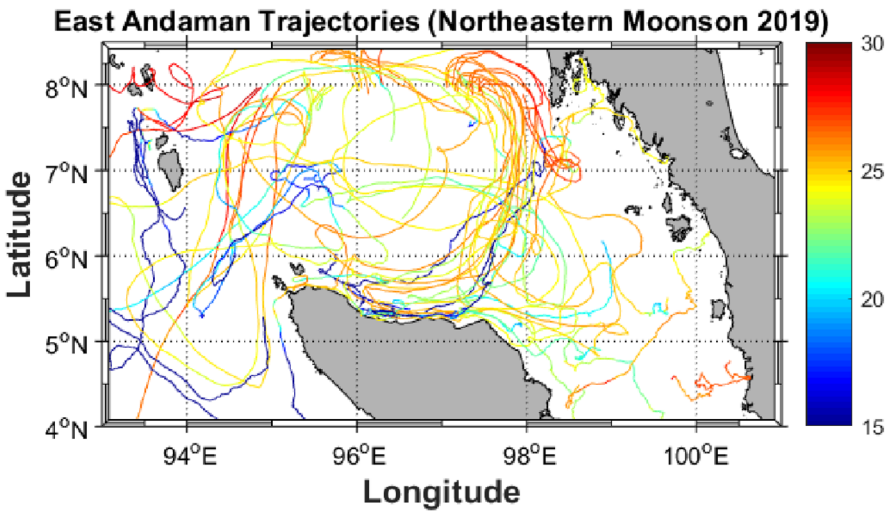

Fig. 9. Simulated trajectories of passive particles in the East Andaman region during the Northeastern Monsoon period from December 2018 to February 2019. The colors represent the age or duration of the particle transport, highlighting the dominant circulation pathways and dispersal patterns in the region.

3.4.2 Southwestern moonson simulation

The filtered particle trajectory simulation for the southwest monsoon in the Andaman Sea revealed a dominant northward movement with distinct rotational patterns : clockwise in the west and counterclockwise in the east. Over time, particles dispersed along the Malay Peninsula, with some stalling along the coastlines, while others formed clockwise eddies in the region. Ultimately, the particles are advected westward into the Indian Ocean or retained

near the Malay Peninsula and Sumatra. This simulation underscores the influence of currents, eddies, and coastal interactions on particle dispersal. Particle temperatures, initially warmer (~30°C) than those during the northeast monsoon, gradually decreased to ~24°C over time.

The Southwest monsoon simulation revealed critical dynamics regarding the fate and transport of particles. The dominant northward movement, combined with westward advection into the Indian Ocean, implies that the Andaman Sea acts as a source region for the export of marine debris and water masses to the wider oceanic basin. Conversely, the observed coastal stall along Sumatra and the Malay Peninsula highlights these areas as high-retention zones that are susceptible to pollutant accumulation. Biologically, the thermal history of the particles, starting at a warm temperature of ~30°C and cooling to ~24°C, suggests that the organisms drifting in these currents experience significant environmental variability. The initial high temperatures may accelerate larval metabolism, while subsequent cooling indicates transport into mixed or distinct water masses, potentially influencing survival rates and connectivity between coastal and offshore ecosystems.

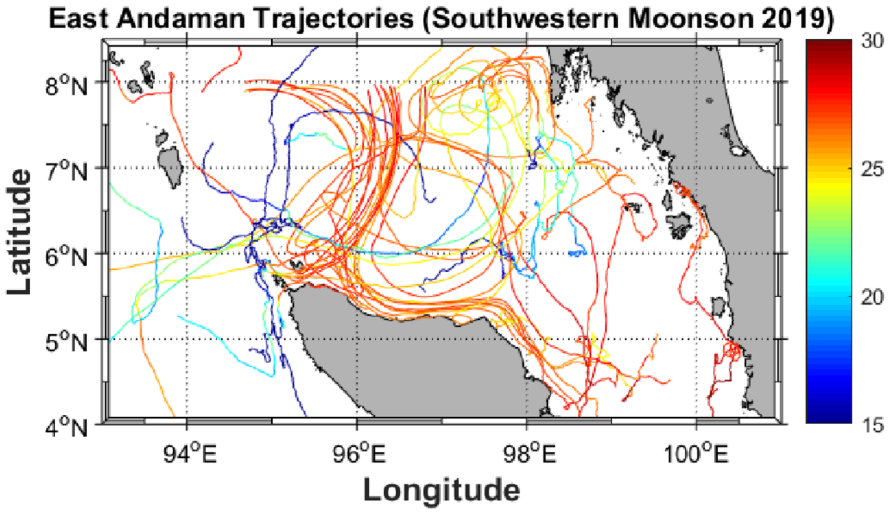

Fig. 10. Simulated trajectories of passive particles in the East Andaman region during the Southwestern Monsoon period from June 2019 to August 2019. The colors represent the age or duration of the particle transport, highlighting the dominant circulation pathways and dispersal patterns in the region.

3.5 Spatial pattern and temporal variability of oceanographic parameters

The spatial pattern of SST variability from EOF analysis was captured by two principal components: mode-1 and mode-2. Mode-1 explained 71.88% of the variance, whereas mode-2 accounted for 16.26%, collectively representing 88.14% of the total variability. This suffices to represent the SST variability at 0.5 a depth. Uniformly negative EOF coefficients across the region indicate spatially homogeneous SST variations. The spatial distribution of EOF mode-1 for SST ranges from –0.9 to –0.05. The Andaman Sea shows the highest variability near 6.8°N, 96.3°E, with a value of –0.9 (**Fig. 11a**). The corresponding principal component (PC) time series for mode-1 (2015–2019) exhibited significant fluctuations (**Fig. 11b**) and was dominated by annual variability. The highest SST occurred in December 2019 and the lowest in May 2016. Spectral analysis (with a 95% confidence interval) revealed significant peaks at 341 days (annual) and 186 d (annual and semi-annual, respectively).

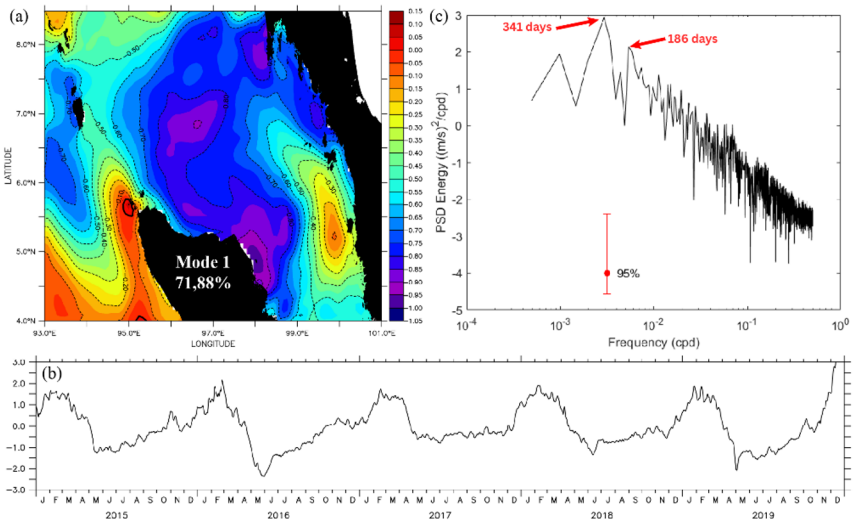

Fig. 11. (a) Spatial pattern of SST derived from Empirical Orthogonal Function (EOF) Mode 1 analysis, (b) the corresponding time-series of the Principal Component (PC), and (c) the Power Spectral Density (PSD) showing dominant frequencies. The analysis identifies key periodicities at 186 and 341 days, representing the secondary mode of SST variability in the region with a 95% confidence interval.

The spatial distribution of SST for EOF mode-2 shows both positive and negative values, ranging from –0.4 to 0.6. The opposing coefficients indicate a dipole pattern. The highest value in the Andaman Sea is 0.2, located near 7.5°N, 94°E (**Fig. 12a**). The corresponding principal component (PC) time series for mode-2 (2015–2019) displayed significant fluctuations (**Fig. 12b**). The temporal pattern of SST EOF mode-2 peaked in November 2019, and reached its lowest value in May 2016. Spectral analysis of the Power Spectral Density (PSD) revealed significant peaks at 292 days (annual), 202 days (semi-annual), and 41 days (annual and semi-annual, respectively).

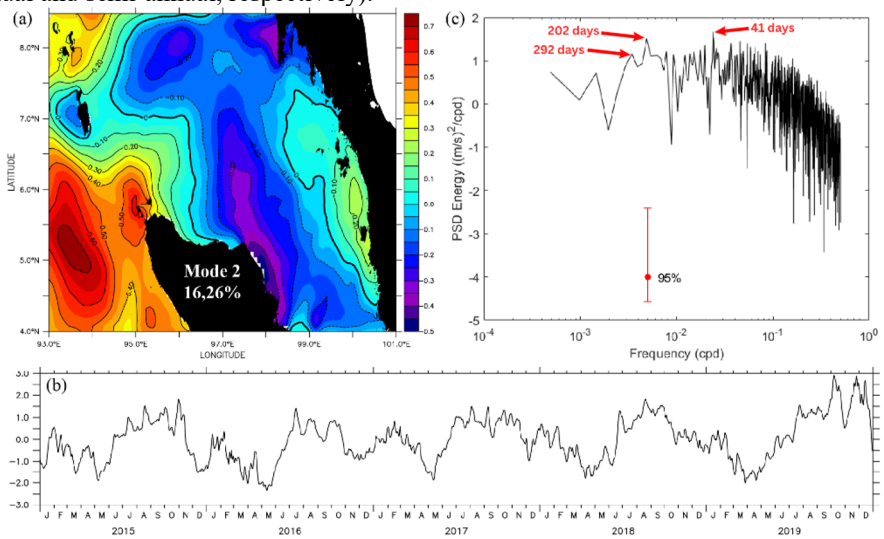

Fig. 12. (a) Spatial pattern of SST derived from Empirical Orthogonal Function (EOF) Mode 2 analysis, (b) the corresponding time-series of the Principal Component (PC), and (c) the Power Spectral Density (PSD) showing dominant frequencies. The analysis identifies key periodicities at 41, 202, and 292 days, representing the secondary mode of SST variability in the region with a 95% confidence interval.

The spatial pattern of salinity variability from the EOF analysis was captured using two principal components: mode-1 and mode-2. Mode-1 explained 71.67% of the variance, whereas mode-2 accounted for 15.35%, collectively representing 87.02% of the total variability. This is sufficient to represent the sea surface salinity variability at 0.5 a depth. The spatial distribution of EOF mode-1 for salinity shows both positive and negative anomalies, ranging from –0.12 to 0.4. The Andaman Sea exhibited high variability, with values reaching 3.5 (**Fig. 13a**). The corresponding principal component (PC) time series for mode-1 (2015 to 2019) fluctuated significantly (**Fig. 13b**) and was dominated by annual variability. The highest salinity occurred in December 2017 and the lowest in March 2015. Peak energy spectral analysis (with a 95% confidence interval) revealed significant periodicities of 341 days (annual) and 186 days (semi-annual).

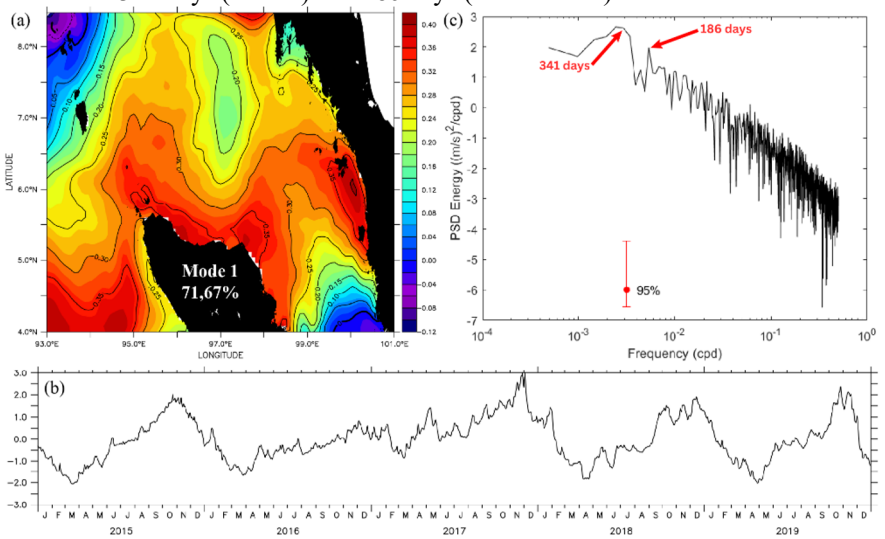

Fig. 13. (a) Spatial pattern of salinity derived from Empirical Orthogonal Function (EOF) Mode 1 analysis, (b) the corresponding /time-series of the Principal Component (PC), and (c) the Power Spectral Density (PSD) showing dominant frequencies. The analysis identifies key periodicities at 186 and 341 days, representing the secondary mode of salinity variability in the region with a 95% confidence interval.

The spatial distribution of salinity for EOF mode-2 exhibited both positive and negative values, ranging from –0.26 to 0.34. The opposing coefficients indicate a dipole pattern. The highest value observed in the Andaman Sea is 0.25 (**Fig. 14a**). The corresponding principal component (PC) time series for mode-2 (2015 – 2019) showed significant fluctuations (**Fig. 14b**) dominated by sub-annual variability. The highest salinity occurred in November 2019, whereas the lowest salinity was recorded in December 2017. Spectral peak analysis of the Power Spectral Density (PSD) revealed significant periodicities at 227 days (sub-annual) and 127 days (intra-seasonal).

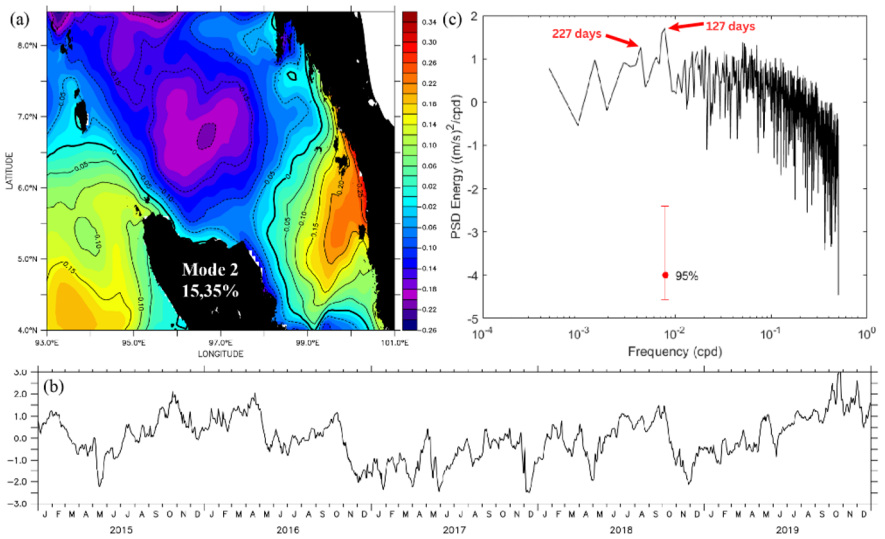

Fig. 14. (a) Spatial pattern of salinity derived from Empirical Orthogonal Function (EOF) Mode 2 analysis, (b) the corresponding time-series of the Principal Component (PC), and (c) the Power Spectral Density (PSD) showing dominant frequencies. The analysis identifies key periodicities at 127 and 227 days, representing the secondary mode of salinity variability in the region with a 95% confidence interval.

3.6 Transport volume

Water mass volume transport was estimated to quantify the flow into and out of the Andaman Sea. Meridional current components were analyzed along a transect connecting Sumatra and the Malay Peninsula (95.5 °E to 101°E, 5.5°N) from the surface to 300 m depth. Time-series data (2015 to 2019) show transport fluctuations ranging from –0.53 Sv (southward) to +1.16 Sv (northward), with a mean of +0.32 Sv. The highest value was recorded in December 2017 (SD = 0.255). During the southwest monsoon, water primarily moves from the Andaman Sea to the Strait of Malacca, while the northeast monsoon reverses this pattern, with stronger inflow from the South China Sea into the Andaman Sea [8].

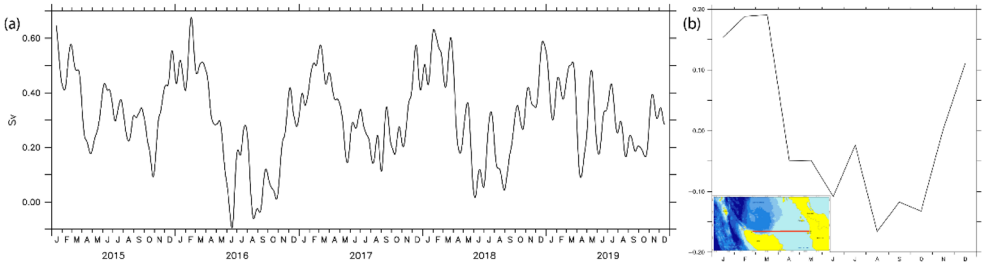

Fig. 15. (a) Time-series of volume transport (Sverdrups, Sv) across the Malacca Strait from 2015 to 2019 and (b) the corresponding monthly climatology anomaly for the upper 300 meters.

4 Conclusion

Summary of findings: This study characterizes the surface circulation of the Andaman Sea, revealing distinct seasonal variability driven by monsoonal forcing that extends to depths of 20 to 70 m. During the Northeast Monsoon, circulation is dominated by northward flow from

the Strait of Malacca toward the Andaman, whereas the Southwest Monsoon drives southward currents from Northern Andaman, resulting in convergence zones and eddy formation. This seasonality is further corroborated by Empirical Orthogonal Function (EOF) analysis; SSH variability is dominated by annual (341 days) and semi-annual (170 days) signals, whereas salinity variability exhibits similar annual periodicity alongside sub-annual and intra-seasonal fluctuations. Lagrangian particle tracking confirms these dynamics, showing that particles circulate locally toward the Andaman region during the Northeast Monsoon but are exported westward into the Indian Ocean during the Southwest Monsoon. The computed average water mass volume transport (0–300 m) for the region was +0.32 Sv.

References

1 A.S. Atmadipoera, G.L. Mubaraq, Struktur dan variabilitas arlindo di Laut Sulawesi. JKN. **11**, 159–174 (2016). https://doi.org/10.15578/jkn.v11i3.6116

2 M. Bayat, H.R. Ahmadi, N. Mahdavi, Application of power spectral density function for damage diagnosis of bridge piers. Struct. Eng. Mech. **71**, 57–63 (2019). https://doi.org/10.12989/sem.2019.71.1.057

3 F.A. Busch, J.D. Niemann, M. Coleman, Evaluation of an empirical orthogonal function-based to downsclae soil moisture patterns based on topographical attributes. Hydrol. Process. **26**, 2696–2709 (2012). https://doi.org/10.1002/hyp.8363

4 S.T. Chandran, S.B. Raj, S. Ravindran, S.V. Narayana, Upper layer circulation, hydrography, and biological response of the Andaman waters during winter monsoon based on in situ and satellite observations. Ocean Dyn. **68**, 801–815 (2018). https://doi.org/10.1007/s10236-018-1160-x

5 S.G. Claudya, Y.I. Siregar, M. Mubarak, The effect of the indian ocean dipole (IOD) phenomenon on oceanographic parameters in the Malacca Strait. AJOAS. **6**, 210–223 (2023)

6 J.R. Curray, Tectonics and history of the Andaman Sea Region. J. Asian Earth Sci. **25**, 187–232 (2005). https://doi.org/10.1016/j.jseaes.2004.09.001

7 J. Hu, J. Gan, Z. Sun, J. Zhu, M. Dai, Observed three-dimensional structure of a cold eddy in the Southwestern South China Sea. J. Geophys. Res. Oceans. **116**, C5 (2011). https://doi.org/10.1029/2010JC006810

8 N.S. Isa, M.F. Akhir, I. Khalil, P.H. Kok, N.H. Roseli, Seasonal characteristics of the sea surface temperature and sea surface currents of Malacca and Andaman Sea. J. Sustain. Sci. Manag. **15**, 66–77 (2020). https://doi.org/10.46754/jssm.2020.06.007

9 N.S. Isa, M.F. Akhir, P.H. Kok, N.R. Daud, I. Khalil, N.H. Roseli, Spatial and temporal variability of sea surface temperature during El-Nino southern oscillation and indian ocean dipole in the Strait of Malacca and Andaman Sea. Reg. Stud. Mar. Sci. **39,** 101402 (2020). https://doi.org/10.1016/j.rsma.2020.101402

10 I. Iskandar, D.O. Lestari, A.D. Saputra, R.Y. Setiawan, A. Wirasatriya, R.D. Susanto, W. Mardiansyah, M. Irfan, Rozirwan, J.D. Setiawan, Kunarso, Extreme positive indian ocean dipole in 2019 and its impact on Indonesia. Sustainability. **14**, 15155 (2022). https://doi.org/10.3390/su142215155

11 D. Jaishree, P.T. Ravichandran, Exploring the upper ocean charactheristics of a bay using coastal and regional ocean community model. Glob. j. environ. sci. manag. **10**, 97–116 (2024). https://doi.org/10.22034/gjesm.2024.01.08

12 I.I. Lestari, S. Nurdiati, A. Sopaheluwakan, Analisis empirical orthogonal function (EOF) berbasis singular value decomposition (SVD) pada data curah hujan Indonesia. JMA. **15**, 13–22 (2016). https://doi.org/10.29244/jmap.15.1.13-22

13 C. Lett, P. Verley, C. Mullon, C. Parada, T. Brochier, P. Penven, B. Blanke, A lagrangian tool for modeling ichtyoplankton dynamics. Environ. Model. Softw. **23**, 1210–1214 (2008). https://doi.org/10.1016/j.envsoft.2008.02.005

14 D.K. Mahapatra, A.D. Rao, Redistribution of low-salinity pools off east coast of India during southwest monsoon season. Estuar. Coast. Shelf Sci. **184**, 21–29 (2017). https://doi.org/10.1016/j.ecss.2016.10.037

15 S. Miladinova, D. Macias, A. Stips, E. Garcia-Gorriz, Identifying distribution and accumulation patterns of floating marine debris in the Black Sea. Mar. Pollut. Bull. **153**, 1–11 (2020). https://doi.org/10.1016/j.marpolbul.2020.110964

16 S. Rizal, P. Damm, M.A. Wahid, J. Sündermann, Y. Ilhamsyah, T. Iskandar, Muhammad, General circulation in the Malacca Strait and Andaman Sea: a numerical model study. Am. J. Environ. Sci. **8**, 479–488 (2012). https://doi.org/10.3844/ajessp.2012.479.488

17 F.T. Tangang, J. Liew, E. Salimun, K.M. Sei. L.J. Le, H. Muhamad, Climate change and variability over Malaysia: gaps in science and research information. Sains Malays. **41**, 1355–1366 (2012)

18 I. Yuwono, W. Rahayu, Akurasi metode concordance berdasarkan panjang tes dan ukuran sampel. JEP. **8**, 1–6 (2017). https://doi.org/10.21009/JEP.081.01

19 M.S. Tarigan, Aplikasi satelit aqua MODIS untuk memprediksi model pemetaan kecerahan air laut di Perairan Teluk Lada, Banten. JMS. **14**, 126131 (2009)

20 I. Iskandar, P.A. Utari, D.O. Lestari, Q.W. Sari, D. Setiabudidaya, M.Y.N. Khakim, I. Yustian, Z. Dahlan, Evolution of 2015/2016 El Nino and its impact on Indonesia, in Proceedings of the AIP Conference, International Symposium on Earth Hazard and Disaster Mitigation (ISEDM) 2016, Bandung, Indonesia, October 11-12 (2017). https://doi.org/10.1063/1.4987095